ELSEVIER

Journal of Chromatography A, 959 (2002) 49–64

JOURNAL OF CHROMATOGRAPHY A

www.elsevier.com/locate/chroma

Stochastic simulation of the partition mechanism with a heterogeneous surface phase

Peter E. Krouskop, Victoria L. McGuffin*

Department of Chemistry, Michigan State University, East Lansing, MI 48824, USA

Received 18 December 2001; received in revised form 9 April 2002; accepted 12 April 2002

Abstract

A three-dimensional stochastic model of chromatography has been used to determine the effect of multiple sites on the partition mechanism. The effect of additional sites on mass transfer rates, zone profiles, and their statistical moments are investigated as a function of the partition coefficient, diffusion coefficient, and interfacial barrier to mass transfer. These studies have demonstrated that changes in the partition coefficient alone are not sufficient to alter the system response from that of a single site. Changes in the diffusion coefficient and the barrier to mass transfer do cause changes in the response compared to that of a single site. The zone profiles produced by the systems become more asymmetric as the difference between the diffusion coefficients or the barriers to mass transfer increases. The site with the slower mass transfer rate plays the dominant role in the total system response.

Keywords: Stochastic simulation; Partition mechanism; Monte Carlo simulation; Absorption mechanism

1. Introduction

Traditionally, chromatography has been studied from two different theoretical approaches. The first approach uses a macroscopic or bulk perspective and applies mass balance equations to determine the eluting solute zone. The second approach uses a microscopic or ensemble perspective and applies probability theory to the random interactions of individual molecules to obtain the elution zone profile. In the long time limit, the two methods have been shown to be equivalent, but each method has provided different insights into the separation process.

The mass balance approach has lead to many interesting insights into the development of the solute zone during the chromatographic process. Taylor [1] and Aris [2] were able to describe the development of a non-retained solute zone in a flowing system. Golshan-Shirazi and Guiochon have reviewed and given four classifications of the many variations of the mass balance approach for retained solutes [3]. Equilibrium-dispersive models [4] assume that the solute is in equilibrium between the fluid and surface phases. All contributions to broadening are included in an apparent dispersion coefficient, usually empirically determined. The kinetic evolution of the system is studied using transport-dispersive and reactive-dispersive models. The transport-dispersive models assume fast kinetics and study the mass transport of the solute between the fluid and surface phases. The reactive-dispersive

*Corresponding author. Tel.: +1-517-255-9715; fax: +1-517-353-1793.

E-mail address: jgshabus@aol.com (V.L. McGuffin).

0021-9673/02/$ – see front matter
PII: S0021-9673(02)00427-2

models assume the mass transfer effects to be negligible and the adsorption/desorption kinetics of the solute at the interface of the fluid and surface phases are investigated [4]. Finally, general rate models [5] allow the study of the interaction of all the processes that are thought to occur within the chromatographic system. To obtain an analytical solution, some aspects of the system may be assumed to be unimportant and omitted from the model. The general rate models have been the basis for studies to determine the statistical moments of the solute zones [6], to establish the relationships between the plate models of chromatography and the mass balance models [7], and to examine of the effects the boundary conditions used to solve the differential equations [8,9]. The mass balance equations have also been solved numerically for cases in which an analytical solution is not possible (e.g., nonlinear chromatography or slow mass transfer) [10]. Recently a mass balance approach has been presented by Gotmar et al. to examine a two-site adsorption system [11]. All of these models provide an understanding of the macroscopic response of chromatographic systems under different conditions.

The second approach to describing the system has been presented by Giddings and Eyring [12]. This approach views the retention process as a series of events that can be described by the laws of statistics. This model is similar to that of statistical mechanics and allows the behavior of individual molecules to determine the system response. The model has been used extensively for adsorption chromatography for one site [12–15] and non-equilibrium systems [16]. A stochastic model that is based on non-equilibrium statistical mechanics has given understanding of the mathematical and physical meanings of dispersion coefficients [17,18]. The stochastic models have also been expanded to incorporate the heterogeneous nature of the surface and mobile phases by Giddings and Eyring [12,13] and McQuarrie [14]. Others have expanded the stochastic model to incorporate multiple adsorption sites into the model [19–21].

Interestingly, no model of heterogeneous phases has been applied to a partition system. Yet, there are many circumstances when the stationary phase may be considered inhomogeneous in partition systems. In some cases, the heterogeneity is introduced intentionally. For example, mixtures of different stationary phases have been used for both gas chromatography [22,23] and liquid chromatography [24–26]. In other cases, the heterogeneity is an unintentional and often undesirable aspect of the system. Such heterogeneities have been found through surface studies of the chromatographic stationary phases. Lochmuller et al. have studied alkyl chain organization on silica supports and found that, for low coverage of the support, the chains tend to group together and form islands [27]. Other studies have examined the selectivity [28] as well as the possibility of phase transitions [29] in stationary phases of different bonding density. Molecular dynamics methods have also been applied to tethered alkyl chains and have shown that the mobile phase as well as the surface phase show inhomogeneities based on radial position [30–36]. Thus, the fluid and surface phases in real partition systems are likely to be heterogeneous. The many different interactions may affect the retention of solute molecules in both beneficial and detrimental ways. Such chromatographic systems are not accurately modeled by assuming a homogenous phase, so interest has moved toward development of appropriate models.

This paper presents a three-dimensional stochastic simulation [37,38] of partition chromatography that has been adapted to allow multiple interactions with a randomly mixed heterogeneous surface. Each surface phase interaction has a defined value for the partition coefficient, diffusion coefficient, and interfacial resistance to mass transfer. The simulation is used to study the effects of multiple surface interactions on the overall system performance of partition chromatography.

2. Simulation

2.1. Description of the program algorithms

A three-dimensional stochastic (Monte Carlo) simulation has been developed that follows the trajectories of individual molecules as they travel through a column consisting of a fluid and surface phase. The simulation models the transport processes of diffusion, laminar or electroosmotic flow, and partition (absorption) [38–40]. These processes are applied to individual molecules at each time incre-

ment t until some total time T is reached. Written in FORTRAN 90, the simulation has been compiled and executed on an IBM RS 6000 workstation.

Recent modifications to the program allow the simulation of multiple surface interactions for the partition mechanism. The number of different types of interaction sites (n) and the relative proportion or probability of encountering those sites in the surface phase (P_i) are input parameters for the simulation. When a fluid-phase molecule intersects the boundary between the fluid and surface phases, a random number (χ) is selected and compared to the relative proportion of the surface sites. The type of surface site (i) is determined when the random number satisfies the relationship:

$$1 - \sum_{j=0}^{n-i} P_{n-j} < \chi \leq \sum_{j=1}^{i} P_j \tag{1}$$

Once the type of site has been chosen, the probability that a molecule will be transferred across the interface is given by the following equations:

$$P_{\mathrm{fs},i} = \mathrm{Min}\left(a_i K_{\mathrm{abs},i} \sqrt{\frac{D_{\mathrm{s},i}}{D_{\mathrm{f}}}}, a_i \right) \tag{2a}$$

and

$$P_{\mathrm{sf},i} = \mathrm{Min}\left(a_i, \frac{a_i}{K_{\mathrm{abs},i}} \sqrt{\frac{D_{\mathrm{f}}}{D_{\mathrm{s},i}}} \right) \tag{2b}$$

where $P_{\mathrm{fs},i}$ is the probability of transfer from the fluid to surface phase and $P_{\mathrm{sf},i}$ is the probability of transfer from the surface to fluid phase for the ith site. The other parameters are D_{f}, the fluid-phase diffusion coefficient, $D_{\mathrm{s},i}$, the surface-phase diffusion coefficient, a_i, the maximum probability for transfer, and K_i, the partition coefficient for the ith site. The maximum probability is used to represent the interfacial resistance to mass transfer between the two phases, and can be related to the activation energy in the Arrhenius equation [38]. Once the appropriate probability has been calculated, a second random number is selected and compared to the calculated probability. If the random number is less than or equal to the calculated value, the appropriate transfer occurs. If the random number is greater than the calculated probability, then no transfer occurs and the molecule undergoes an elastic collision with the interface. This approach results in completely independent interactions for the molecule each time the interface is encountered.

2.2. Description of the program output

The results of the simulation are used to characterize mass transfer between the phases and to produce zone profiles with the corresponding statistical moments in both time and distance. Mass transfer curves, like that shown in Fig. 1, are obtained by starting all molecules in the fluid phase and allowing the system to progress over time to a steady-state distribution. The number of molecules in each phase is recorded as a function of simulation time. The mass transfer rate constants from the fluid to surface phase (k_{fs}) and from the surface to fluid phase (k_{sf}) are determined by fitting the data to the kinetic equation for a first-order reversible reaction:

$$\frac{N_{\mathrm{f}}}{N} = \frac{\left[k_{\mathrm{sf}} + k_{\mathrm{fs}} \exp\{ -(k_{\mathrm{fs}} + k_{\mathrm{sf}})T \} \right]}{k_{\mathrm{fs}} + k_{\mathrm{sf}}} \tag{3}$$

where N_{f} is the number of molecules in the fluid phase, N is the total number of molecules, and T is the time elapsed in the simulation [41]. The kinetic curves are also used to determine the characteristic times at which the system achieves 50% (T_{50}), 90%

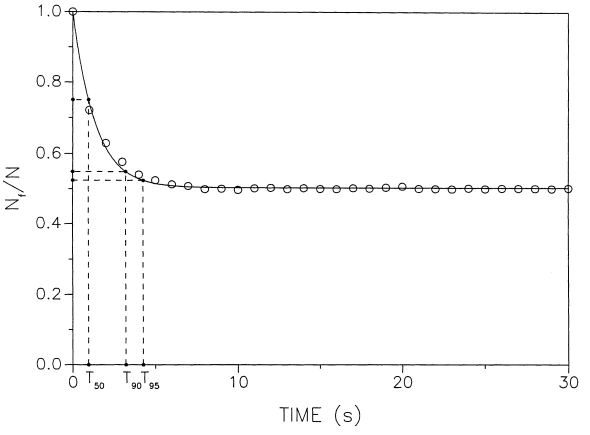

Fig. 1. Mass transfer decay curve (○) and the characteristic times representing 50% (T_{50}), 90% (T_{90}), and 95% (T_{95}) of the net change of fluid-phase molecules. (—) Fit of Eq. (3) to the data: $k_{\mathrm{fs}} = 0.366 \pm 0.003\ \mathrm{s}^{-1}$ and $k_{\mathrm{sf}} = 0.371 \pm 0.005\ \mathrm{s}^{-1}$ ($R^2 = 0.966$). Simulation conditions: $N = 10\,000$; $t = 1.0 \cdot 10^{-3}$ s; $R_{\mathrm{f}} = 2.0 \cdot 10^{-3}$ cm; $R_{\mathrm{s}} = 8.28 \cdot 10^{-4}$ cm; $D_{\mathrm{f}} = 1.0 \cdot 10^{-5}\ \mathrm{cm}^2\ \mathrm{s}^{-1}$; $D_{\mathrm{s}} = 1.0 \cdot 10^{-7}\ \mathrm{cm}^2\ \mathrm{s}^{-1}$; $K = 1.0$; $a = 1.0$.

(T_{90}), and 95% (T_{95}) of the change between the initial and steady-state conditions (Fig. 1). It is also possible to obtain the average number of molecules in the fluid ($\tilde{N}_f$) and surface ($\tilde{N}_s$) phases at steady state from these data. The kinetic and steady-state behavior of the system is related in the following manner:

$$\frac{k_{fs}}{k_{sf}} = \frac{\tilde{N}_s}{\tilde{N}_f} = k = K\beta \tag{4}$$

where k is the capacity factor, K the the effective partition coefficient, and β is the ratio of the surface-phase volume $[V_s = \pi\{(R_f + R_s)^2 - R_f^2\}L]$ to the fluid-phase volume ($V_f = \pi R_f^2 L$).

Zone profiles in distance can be obtained by creating a histogram of the axial positions of the solute molecules at specified times and smoothing the resulting profile using fast Fourier techniques [38–40]. Zone profiles in time are similarly obtained from a histogram of the elution times of the molecules at specified distances. The data are also used to obtain statistical moments for the profiles in both distance and time. The moments are calculated as follows:

$$M_1(x) = \frac{\sum_{i=1}^{N} x_i}{N} \tag{5}$$

$$M_n(x) = \frac{\sum_{i=1}^{N} (x_i - M_1)^n}{N} \tag{6}$$

where M_n are the central moments, and x_i is a datum from the time or distance domain. The first moment (M_1) represents the mean value, the second moment (M_2) is the variance, and the third moment (M_3) is related to the asymmetry of the profile.

3. Results

In this work, the stochastic simulation is used to study the effects of multiple partition pathways on the chromatographic process. The system studied is an open tubular column with a fluid-phase radius of $2.0 \cdot 10^{-3}$ cm and a surface-phase film thickness of $8.24 \cdot 10^{-4}$ cm. These values are used so that the volume phase ratio β is equal to 1.0. The system contains two partition pathways that are used to study the overall effects of differences in partition coefficient (K_i), surface-phase diffusion coefficient ($D_{s,i}$), and interfacial resistance to mass transfer coefficient (a_i). The simulation is performed for a total time necessary for all molecules to elute from column lengths of 0.1, 0.3, 0.5, 1.0, 3.0, and 5.0 cm. During the simulation time, distance data are collected at 5 s intervals. The observed kinetics of the system, chromatographic zone profiles, and statistical moments are presented and discussed below.

3.1. Effect of differences in the partition coefficient

To explore the effects of differing partition coefficients, a series of systems is simulated in which the average partition coefficient is held constant, while the difference between the values is varied. The average partition coefficient is determined by $K_{avg} = P_1K_1 + P_2K_2$, where K_1 and K_2 are the respective partition coefficients. With a probability of 0.5 for each type of surface interaction, the ratio $(K_2 - K_1)/K_{avg}$ was varied while holding K_{avg} constant at a value of 1.0. The steady-state and kinetic data for these systems as well as for a single site with a partition coefficient of 1.0 are presented at the top of Table 1. The ratio of the number of molecules in the surface and fluid phases ($\tilde{N}_s/\tilde{N}_f$) indicates that the steady-state distribution for these systems is similar and is determined by the average partition coefficient (Eq. (4)). The mass transfer curves for these systems are fit to Eq. (3) by using nonlinear regression. The acquired kinetic rate constants for mass transfer are approximately equal for all four systems. The degree of fit to Eq. (3), as shown by the square of the correlation coefficient (R^2), is comparable for all four systems as well. The ratio of the mass transfer rate constants (k_{fs}/k_{sf}) is also equal to the average partition coefficient. The values of the characteristic times T_{50}, T_{90}, and T_{95} are also similar. This implies that these four systems, which have the same average partition coefficient, are equivalent. In fact, the rate constants, R^2 values, and characteristic times are all statistically equal at the 95% confidence level.

To further test this phenomenon, three systems are simulated such that the ratio $(K_2 - K_1)/K_{avg}$ is constant with a value of 1.0 and K_{avg} is varied from 0.5

Table 1
Rate constants (k_{fs}, k_{sf})[a], characteristic times (T_{50}, T_{90}, T_{95}), and steady-state distributions ($\tilde{N}_s/\tilde{N}_f$) for mass transfer processes as a function of partition coefficient and probability of partition sites[b]

K_1	K_2	P_1	P_2	$\tilde{N}_s/\tilde{N}_f$	k_{fs}/k_{sf}	k_{fs} (s^{-1})	k_{sf} (s^{-1})	R^2	T_{50} (s)	T_{90} (s)	T_{95} (s)
1.0	–	1.0	–	0.995±0.002	0.988±0.005	0.366±0.003	0.371±0.005	0.966±0.001	0.74±0.02	3.63±0.08	4.9±0.2
1.0	1.0	0.5	0.5	1.008±0.005	0.992±0.003	0.370±0.006	0.373±0.006	0.965±0.001	0.75±0.01	3.93±0.09	5.3±0.2
0.75	1.25	0.5	0.5	1.002±0.002	0.991±0.002	0.370±0.003	0.374±0.003	0.965±0.002	0.74±0.01	3.79±0.09	5.0±0.1
0.5	1.5	0.5	0.5	0.995±0.002	0.986±0.002	0.367±0.004	0.372±0.004	0.967±0.001	0.75±0.02	3.74±0.07	5.2±0.2
0.5	–	1.0	–	0.499±0.001	0.498±0.002	0.183±0.002	0.367±0.006	0.973±0.002	1.06±0.02	4.8±0.1	6.7±0.4
0.25	0.75	0.5	0.5	0.499±0.001	0.497±0.002	0.179±0.002	0.359±0.005	0.974±0.002	1.10±0.01	4.9±0.1	6.2±0.1
1.0	–	1.0	–	0.995±0.002	0.988±0.005	0.366±0.003	0.371±0.005	0.966±0.001	0.74±0.02	3.63±0.08	4.9±0.2
0.5	1.5	0.5	0.5	0.995±0.002	0.986±0.002	0.367±0.004	0.372±0.004	0.967±0.001	0.75±0.02	3.74±0.07	5.2±0.2
5.0	–	1.0	–	4.98±0.02	4.38±0.02	2.17±0.01	0.495±0.004	0.898±0.003	0.174±0.003	1.52±0.04	2.31±0.04
2.5	7.5	0.5	0.5	5.03±0.03	4.36±0.03	2.20±0.03	0.506±0.008	0.896±0.001	0.172±0.002	1.52±0.03	2.28±0.04
1.0	1.0	0.5	0.5	1.008±0.005	0.992±0.003	0.370±0.006	0.373±0.006	0.965±0.001	0.75±0.01	3.93±0.09	5.3±0.2
0.1	10.0	0.909	0.091	0.988±0.003	0.988±0.008	0.365±0.006	0.369±0.009	0.965±0.003	0.74±0.02	3.73±0.06	4.98±0.04
0.01	10.0	0.901	0.099	0.990±0.004	0.983±0.001	0.372±0.004	0.378±0.004	0.963±0.002	0.723±0.003	3.76±0.08	5.1±0.1

[a] Determined by nonlinear regression according to Eq. (3) with square of the correlation coefficient R^2.
[b] Simulation conditions: $N=10\,000$; $t=1.0\cdot10^{-3}$ s; $T=20\tau$; $R_f=2.0\cdot10^{-3}$ cm; $R_s=8.28\cdot10^{-4}$ cm; $D_f=1.0\cdot10^{-5}$ cm^2 s^{-1}; $D_{s,1}=D_{s,2}=1.0\cdot10^{-7}$ cm^2 s^{-1}; $a_1=a_2=1.0$.

to 5.0. Corresponding systems with a single site are also presented for comparison. The steady-state behavior ($\tilde{N}_s/\tilde{N}_f$) of the multiple-site systems is the same as the corresponding single-site systems, as seen in the middle of Table 1. The kinetic behavior of the multiple-site systems is also equivalent to that of the single-site systems. The rate constants, R^2 values, and characteristic times for these systems are statistically equal at the 95% confidence level.

Finally, the partition coefficients and probabilities of each site are varied while holding K_{avg} at a constant value of 1.0. The steady-state and kinetic behavior of these systems is statistically identical to the others with a value of 1.0 for K_{avg}, as seen at the bottom of Table 1. Even the system in which the partition coefficients differ by three orders of magnitude does not deviate from the observed trend. Thus, it appears that the systems truly behave as a system with a single site having a partition coefficient equal to K_{avg}. This suggests that the kinetics of the overall system cannot be used to determine the number of sites or the strength of their interaction with the solute if the only difference between the sites is the partition coefficient.

To further study the effects of the partition coefficient, the fluid dynamic behavior of the systems at the top of Table 1 is simulated with a fluid-phase velocity (v) of 0.1 cm s^{-1}. The zone profiles produced at column lengths from 0.1 to 5.0 cm are shown in Fig. 2. It can be seen that the three systems appear similar. This is the result of the similar mass transfer kinetics and equilibrium behavior seen previously in Table 1. The maxima of the zone profiles at each column length occur at the same point in time and have the same magnitude for all three systems. The first two profiles show a large front followed by a very small tail that grows and can be easily seen in the third and fourth profiles. The tail then diminishes as the last two zone profiles become symmetric.

The systems discussed above can be quantitatively compared by means of the statistical moments of the zone profiles. The moments were calculated in time and distance using Eqs. (5) and (6). Fig. 3A displays the first moment in time, or mean elution time, at each column length, and Fig. 4A shows the corresponding first moment in distance, or mean zone position. The first moments in time and distance are linear and equal in magnitude. The linearity of the first moments in both domains implies that the systems are at steady state. The fact that the systems are equal in magnitude indicates that the systems are

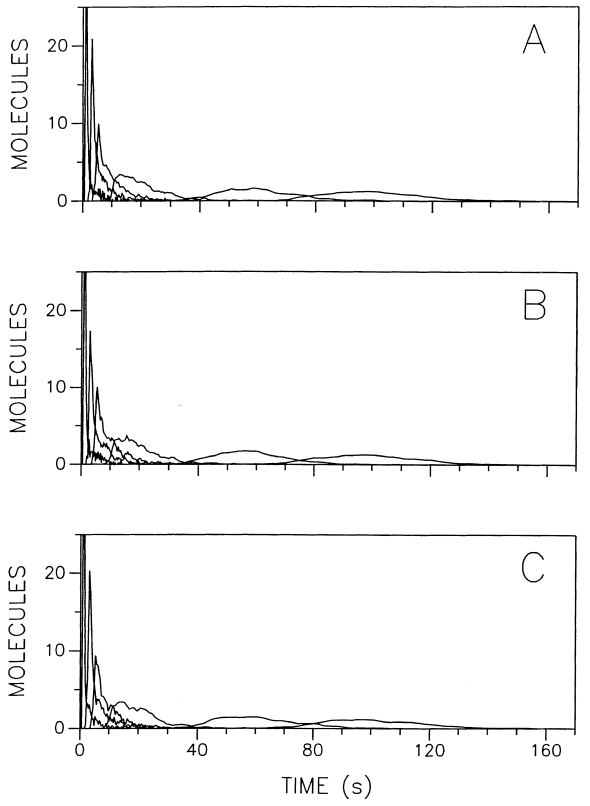

Fig. 2. Zone profiles for systems with laminar flow and two partition sites with (A) $K_1 = K_2 = 1.0$; (B) $K_1 = 0.75$, $K_2 = 1.25$; (C) $K_1 = 0.5$, $K_2 = 1.5$. Simulation conditions: $N = 1000$; $t = 5.0 \cdot 10^{-5}$ s; $R_f = 2.0 \cdot 10^{-3}$ cm; $R_s = 8.28 \cdot 10^{-4}$ cm; $L = 0.1$, 0.2, 0.5, 1.0, 2.0, and 5.0 cm; $v = 0.1$ cm s^{-1}; $D_f = 1.0 \cdot 10^{-5}$ cm^2 s^{-1}; $D_{s,1} = D_{s,2} = 1.0 \cdot 10^{-7}$ cm^2 s^{-1}; $P_1 = P_2 = 0.5$; $a_1 = a_2 = 1.0$.

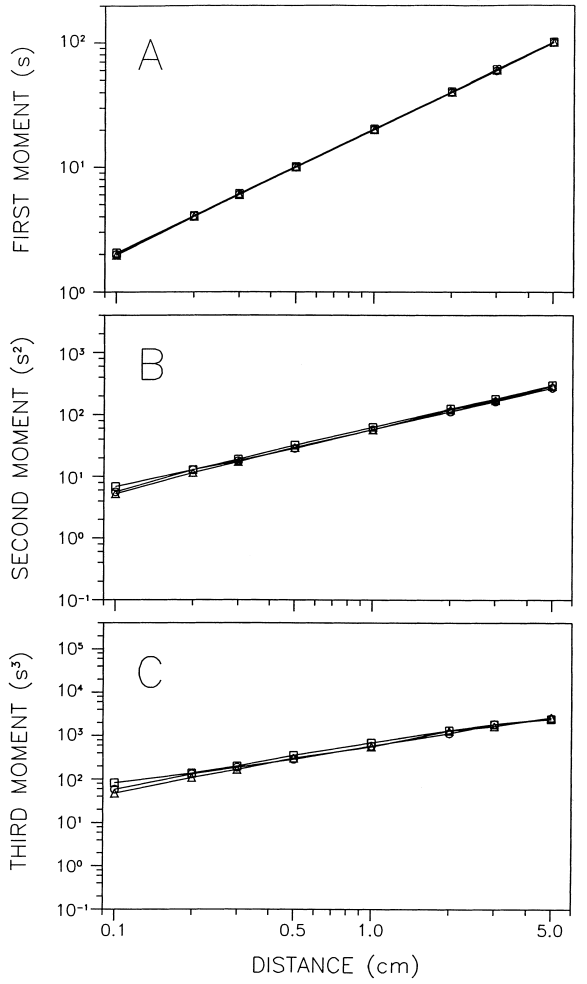

Fig. 3. The calculated (A) first moment, (B) second moment, and (C) third moment in time as a function of distance for systems with (△) $K_1 = K_2 = 1.0$; (○) $K_1 = 0.75$, $K_2 = 1.25$; (□) $K_1 = 0.5$, $K_2 = 1.5$. All other conditions as in Fig. 2.

independent of the changes in partition coefficient. The slope of the first moment in either the time or distance domain is related to the partition coefficient as shown below for a system with a single site at steady state:

$$M_{1,t} = \frac{(1 + K\beta)}{v} L \tag{7}$$

$$M_{1,l} = \frac{v}{(1 + K\beta)} T \tag{8}$$

Eq. (7) shows the relationship between the first moment in time as a function of distance (L), velocity (v), and volume phase ratio (β). Eq. (8) shows the corresponding relationship between the first moment in distance as a function of time (T). The first moments of these systems all have the same slope in Figs. 3A and 4A, implying that the systems have the same average partition coefficient. The overall response of each system is equivalent to a system with a single site having the same partition coefficient. In these graphs, the observed equivalent partition coefficient is equal to 1.0. This leads to the conclusion that differences in the partition coefficient of the sites on the surface is not sufficient to cause a difference in the mean response of the system.

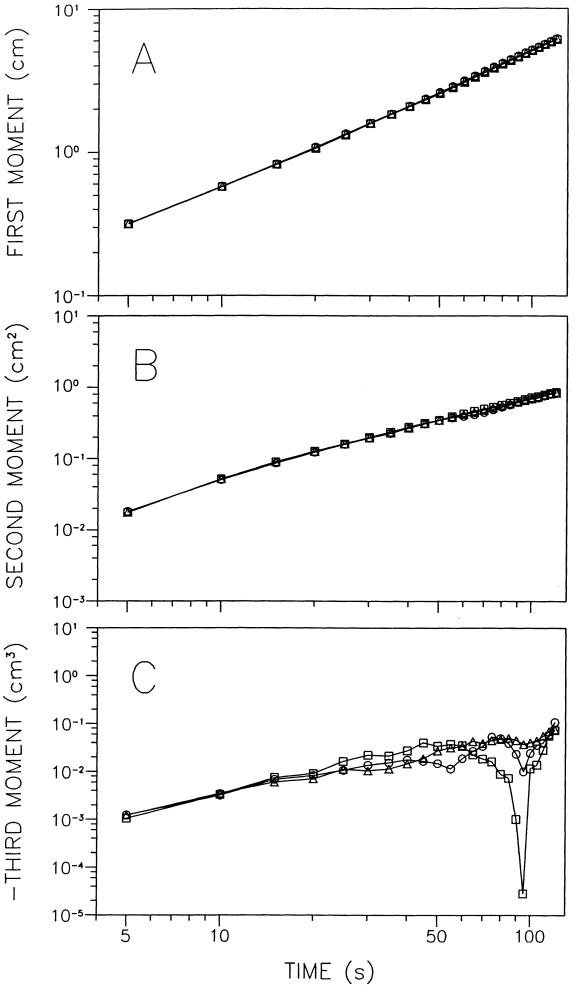

Fig. 4. The calculated (A) first moment, (B) second moment, and (C) third moment in distance as a function of time for systems with (△) $K_1 = K_2 = 1.0$; (○) $K_1 = 0.75$, $K_2 = 1.25$; (□) $K_1 = 0.5$, $K_2 = 1.5$. All other conditions as in Fig. 2.

Figs. 3B and 4B show the second moment or variance in time and distance, respectively. The data in Fig. 3B are linear and show small differences in variance at short distances that disappear as distance increases. In Fig. 4B, the moments are linear and show no difference in variance between the systems. These observations imply that the variance of the profiles is not affected by the differences in the partition coefficients of the two sites. For a system with a single site at steady state, the variance can be calculated by the modified equation of Golay [6]:

$$M_{2,t} = \left[\frac{2D_f}{v^3} + \frac{2K\beta D_s}{v^3} + \frac{\{1 + 6K\beta + 11(K\beta)^2\}R_f^2}{24(1 + K\beta)^2 D_f v} + \frac{2K\beta R_s^2}{3(1 + K\beta)^2 D_s v} \right] L \quad (9)$$

$$M_{2,l} = \left[\frac{2D_f}{(1 + K\beta)} + \frac{2K\beta D_s}{(1 + K\beta)} + \frac{\{1 + 6K\beta + 11(K\beta)^2\}R_f^2 v^2}{24(1 + K\beta)^3 D_f} + \frac{2K\beta R_s^2 v^2}{3(1 + K\beta)^3 D_s} \right] T \quad (10)$$

Eq. (9) shows the relationship between the partition coefficient and the second moment in time as a function of distance. The relationship between the second moment in distance as a function of time and the partition coefficient is shown in Eq. (10). The first two terms of Eqs. (9) and (10) represent diffusional broadening in the fluid and surface phases, whereas the last two terms represent resistance to mass transfer in the fluid and surface phases. Thus, changes in the partition coefficient would be expected to cause changes in the amount of broadening produced by the systems. The linearity of the graphs indicates that the steady-state conditions of the Golay equation are applicable to the systems. The common line shared by the systems in each graph confirms that the mass transfer within the different systems is equivalent because the average partition coefficient is the same.

The third moments in time and distance are displayed in Figs. 3C and 4C, respectively. The third moments in both time and distance increase linearly and are similar in magnitude for all systems. These observations indicate that the systems are at steady state and the asymmetry is not dependent on the different partition coefficients. The third moments in time as a function of distance are positive, while the third moments in distance as a function of time are negative because zone profiles that are tailing in one domain are fronting in the other.

The fluid dynamic behavior of these systems, as presented in the zone profiles and moments, do not show any dependence on the difference in the partition coefficient between the two sites. The

systems behave identically to a system having a single site with the same average partition coefficient. This is in agreement with the kinetic observations presented earlier.

3.2. Effect of differences in the diffusion coefficient

The simulation is used to study the effects of two different surface-phase diffusion coefficients on the mass transfer rate and the zone profiles of multiple-site partition systems. The diffusion coefficient of one surface site is $1.0\cdot10^{-7}$ cm^2 s^{-1}, and the diffusion coefficient of the other site is varied from $1.0\cdot10^{-5}$ to $1.0\cdot10^{-8}$ cm^2 s^{-1}. All other parameters remain constant. The steady-state distribution of molecules between the fluid and surface phases ($\tilde{N}_s/\tilde{N}_f$) in Table 2 is independent of the changes in diffusion coefficient and, as expected, is equal to 1.0 for these systems. However, the mass transfer rate constants in Table 2 vary from 2.6 s^{-1} for the largest diffusion coefficient to 0.129 s^{-1} for the smallest diffusion coefficient of the second site. The degree of fit with Eq. (3) is best for the systems where the diffusion coefficients of the two sites are equal ($D_{s,1}=D_{s,2}=1.0\cdot10^{-7}$ cm^2 s^{-1}). The larger the difference in the diffusion coefficients, the lower the R^2 value because the system response no longer appears to be a single exponential decay. The characteristic times are useful in observing the trend toward two independent rates of transfer across the phase boundary of the system. The changes in T_{50}, T_{90}, and T_{95} indicate that the larger diffusion coefficient controls the short-time behavior and the smaller diffusion coefficient controls the long-time behavior of these systems. Based on these kinetic data, it is expected that changes in the diffusion coefficient will affect the fluid dynamic behavior of the system.

The effects of the changes in the mass transfer rate can be easily seen in the zone profiles of the systems. Fig. 5 shows the zone profiles for the systems presented in Table 2 at columns lengths of 0.1 to 5.0 cm. The height of the profiles decreases and the width increases as the column length increases for all the systems. It is also noticeable that the profiles at the longest column length become wider and shorter as the diffusion coefficient of the second site decreases. The increase in width is predicted by chromatographic theory for a single site (Eqs. (9) and (10)) [6], and the decrease in height occurs because the area remains constant (i.e., there is no change in the number of solute molecules). Also, the first four profiles for each system are noticeably asymmetric. The asymmetry decreases as the column length increases. For a fixed column length, the asymmetry also decreases as the diffusion coefficient of the second site increases.

The statistical moments for the zone profiles in time and distance are presented in Figs. 6 and 7, respectively. Two series of systems are presented. In one series, which has already been shown in Table 2 and Fig. 5, the diffusion coefficient of the first site is held constant at $1.0\cdot10^{-7}$ cm^2 s^{-1} and the diffusion coefficient of the second site is varied from $1.0\cdot10^{-5}$ to $1.0\cdot10^{-8}$ cm^2 s^{-1}. In the other series, the diffusion coefficient of the first site is held constant at $1.0\cdot10^{-6}$ cm^2 s^{-1} and the diffusion coefficient of the second site ranges from $1.0\cdot10^{-5}$ to $1.0\cdot10^{-8}$ cm^2 s^{-1}. The first moments in time as a function of distance shown in Fig. 6A are linear and equal in magnitude. These observations again imply that the

Table 2
Rate constants (k_{fs}, k_{sf})[a], characteristic times (T_{50}, T_{90}, T_{95}), and steady-state distributions ($\tilde{N}_s/\tilde{N}_f$) for mass transfer processes as a function of diffusion coefficient[b]

$D_{s,1}$ (cm^2 s^{-1})	$D_{s,2}$ (cm^2 s^{-1})	$\tilde{N}_s/\tilde{N}_f$	k_{fs}/k_{sf}	k_{fs} (s^{-1})	k_{sf} (s^{-1})	R^2	T_{50} (s)	T_{90} (s)	T_{95} (s)
$1.0\cdot10^{-7}$	$1.0\cdot10^{-5}$	0.992±0.004	0.960±0.002	2.51±0.07	2.61±0.07	0.43±0.01	0.042±0.003	2.41±0.03	3.75±0.05
$1.0\cdot10^{-7}$	$1.0\cdot10^{-6}$	0.987±0.003	0.973±0.002	1.16±0.03	1.20±0.03	0.82±0.02	0.190±0.002	2.1±0.1	3.8±0.1
$1.0\cdot10^{-7}$	$1.0\cdot10^{-7}$	1.008±0.005	0.992±0.003	0.370±0.006	0.373±0.006	0.965±0.001	0.75±0.01	3.9±0.1	5.3±0.2
$1.0\cdot10^{-7}$	$1.0\cdot10^{-8}$	0.996±0.004	0.972±0.007	0.129±0.002	0.133±0.003	0.780±0.004	1.83±0.03	26±3	46±3

[a] Determined by nonlinear regression according to Eq. (3) with square of the correlation coefficient R^2.
[b] Simulation conditions: $N=10\,000$; $t=1.0\cdot10^{-3}$ s; $T=20\tau$; $R_f=2.0\cdot10^{-3}$ cm; $R_s=8.28\cdot10^{-4}$ cm; $D_f=1.0\cdot10^{-5}$ cm^2 s^{-1}; $P_1=P_2=0.5$; $K_1=K_2=1.0$; $a_1=a_2=1.0$.

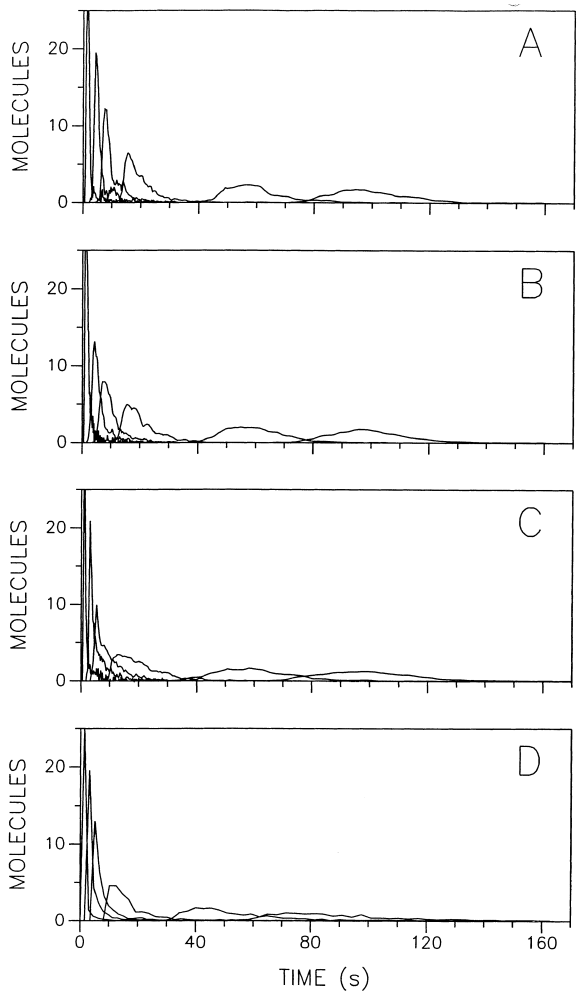

Fig. 5. Zone profiles for systems with laminar flow and two partition sites with (A) $D_{s,1}=1.0\cdot10^{-5}$ cm^2 s^{-1}, $D_{s,2}=1.0\cdot10^{-7}$ cm^2 s^{-1}; (B) $D_{s,1}=1.0\cdot10^{-6}$ cm^2 s^{-1}, $D_{s,2}=1.0\cdot10^{-7}$ cm^2 s^{-1}; (C) $D_{s,1}=1.0\cdot10^{-7}$ cm^2 s^{-1}, $D_{s,2}=1.0\cdot10^{-7}$ cm^2 s^{-1}; (D) $D_{s,1}=1.0\cdot10^{-8}$ cm^2 s^{-1}, $D_{s,2}=1.0\cdot10^{-7}$ cm^2 s^{-1}. Simulation conditions: $N=1000$; $t=5.0\cdot10^{-5}$ s; $R_f=2.0\cdot10^{-3}$ cm; $R_s=8.28\cdot10^{-4}$ cm; $L=0.1$, 0.2, 0.5, 1.0, 2.0, and 5.0 cm; $v=0.1$ cm s^{-1}; $D_f=1.0\cdot10^{-5}$ cm^2 s^{-1}; $P_1=P_2=0.5$; $K_1=K_2=1.0$; $a_1=a_2=1.0$.

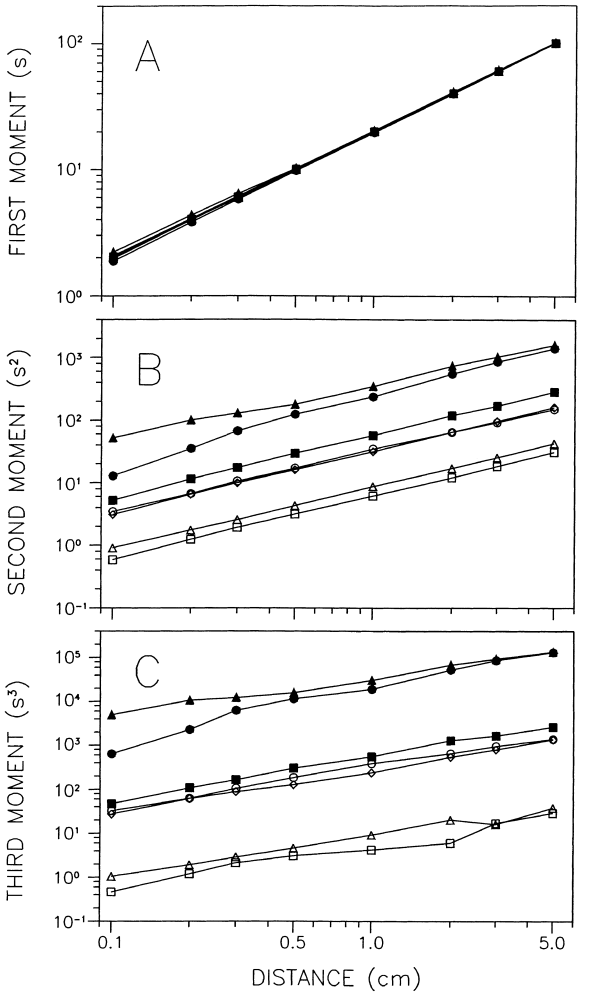

Fig. 6. The calculated (A) first moment, (B) second moment, and (C) third moment in distance as a function of time for systems with (□) $D_{s,1}=1.0\cdot10^{-5}$ cm^2 s^{-1}, $D_{s,2}=1.0\cdot10^{-6}$ cm^2 s^{-1}; (○) $D_{s,1}=1.0\cdot10^{-5}$ cm^2 s^{-1}, $D_{s,2}=1.0\cdot10^{-7}$ cm^2 s^{-1}; (△) $D_{s,1}=1.0\cdot10^{-6}$ cm^2 s^{-1}, $D_{s,2}=1.0\cdot10^{-6}$ cm^2 s^{-1}; (◇) $D_{s,1}=1.0\cdot10^{-6}$ cm^2 s^{-1}, $D_{s,2}=1.0\cdot10^{-7}$ cm^2 s^{-1}; (●) $D_{s,1}=1.0\cdot10^{-6}$ cm^2 s^{-1}, $D_{s,2}=1.0\cdot10^{-8}$ cm^2 s^{-1}; (■) $D_{s,1}=1.0\cdot10^{-7}$ cm^2 s^{-1}, $D_{s,2}=1.0\cdot10^{-7}$ cm^2 s^{-1}; (▲) $D_{s,1}=1.0\cdot10^{-7}$ cm^2 s^{-1}, $D_{s,2}=1.0\cdot10^{-8}$ cm^2 s^{-1}. All other conditions as in Fig. 5.

movement of the zones has reached steady state and that the different mass transfer rates have no effect on the average system response. The first moments in distance as a function of time in Fig. 7A show a different result. While the first moments are linear, they are not equal in magnitude. The first moments in distance increase as the diffusion coefficient of the second site decreases. The observed separation of first moments is the result of different rates of zone movement through the system. The deviations, easily seen in Fig. 7A for the diffusion coefficient combinations of $D_{s,1}=1.0\cdot10^{-6}$ and $D_{s,2}=1.0\cdot10^{-8}$ cm^2 s^{-1} or $D_{s,1}=1.0\cdot10^{-7}$ and $D_{s,2}=1.0\cdot10^{-8}$ cm^2 s^{-1} can best be described by the slow kinetics of mass transfer observed for these systems (Table 2). The

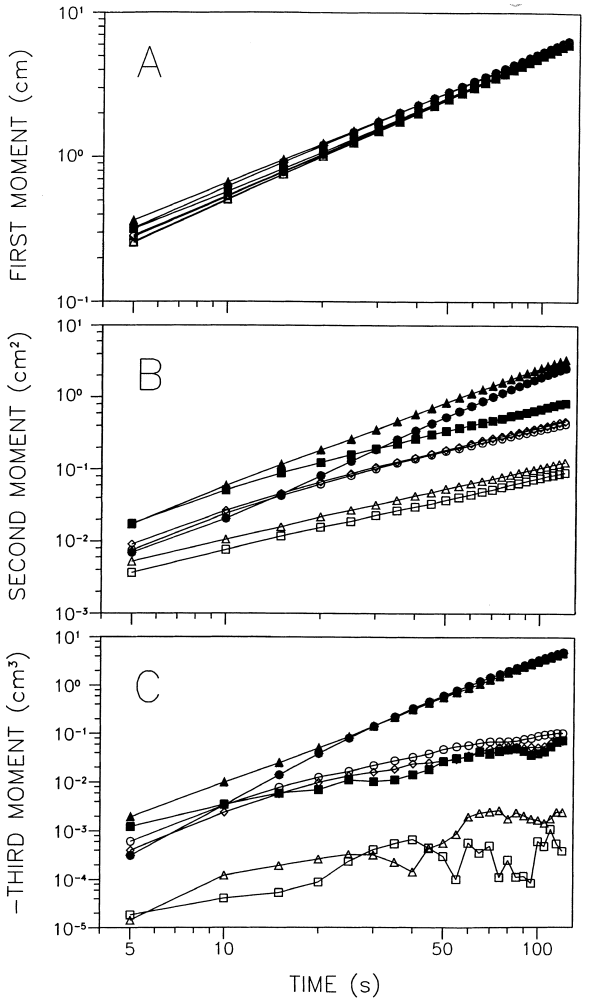

Fig. 7. The calculated (A) first moment, (B) second moment, and (C) third moment in time as a function of distance for systems with (□) $D_{s,1}=1.0\cdot10^{-5}$ cm^2 s^{-1}, $D_{s,2}=1.0\cdot10^{-6}$ cm^2 s^{-1}; (○) $D_{s,1}=1.0\cdot10^{-5}$ cm^2 s^{-1}, $D_{s,2}=1.0\cdot10^{-7}$ cm^2 s^{-1}; (△) $D_{s,1}=1.0\cdot10^{-6}$ cm^2 s^{-1}, $D_{s,2}=1.0\cdot10^{-6}$ cm^2 s^{-1}; (◇) $D_{s,1}=1.0\cdot10^{-6}$ cm^2 s^{-1}, $D_{s,2}=1.0\cdot10^{-7}$ cm^2 s^{-1}; (●) $D_{s,1}=1.0\cdot10^{-6}$ cm^2 s^{-1}, $D_{s,2}=1.0\cdot10^{-8}$ cm^2 s^{-1}; (■) $D_{s,1}=1.0\cdot10^{-7}$ cm^2 s^{-1}, $D_{s,2}=1.0\cdot10^{-7}$ cm^2 s^{-1}; (▲) $D_{s,1}=1.0\cdot10^{-7}$ cm^2 s^{-1}, $D_{s,2}=1.0\cdot10^{-8}$ cm^2 s^{-1}. All other conditions as in Fig. 5.

solute molecules were all started in the mobile phase and, because of the slow kinetics to enter the surface phase, the velocity of the solute zone is faster than the steady-state velocity. The zone then travels farther down the column than expected from equilibrium theories. As the system relaxes over time, a steady state is established and the average velocity of the molecules approaches that predicted by theory. However, there is a constant offset in the first moment due to the initial period of non-equilibrium. Longer periods of non-equilibrium associated with smaller diffusion coefficients of the second site produce larger offsets as seen in Fig. 7A.

The second moment or variance in time as a function of distance is shown in Fig. 6B. The graphs are linear but vary in magnitude and can be separated into three distinct groups. The systems with a value of $1.0\cdot10^{-6}$ cm^2 s^{-1} for the smallest diffusion coefficient have the fastest mass transfer rates and, correspondingly, the smallest values of the second moment. Systems with a value of $1.0\cdot10^{-7}$ cm^2 s^{-1} for the smallest diffusion coefficient appear in the middle of the graph, indicating that the zones have broadened more due to the slower mass transfer rates. The systems with the largest second moments have a diffusion coefficient of $1.0\cdot10^{-8}$ cm^2 s^{-1}. These results suggest that the systems behave as if limited by the smallest diffusion coefficient. The larger diffusion coefficient of the pair does not change the system response appreciably at long distances. However at short distances, the site with the larger diffusion coefficient does influence the system response, as seen for the systems with $D_{s,1}=1.0\cdot10^{-6}$ and $D_{s,2}=1.0\cdot10^{-8}$ cm^2 s^{-1} or $D_{s,1}=1.0\cdot10^{-7}$ and $D_{s,2}=1.0\cdot10^{-8}$ cm^2 s^{-1}. Fig. 7B shows the variance in distance as a function of time for these systems. Some of the general trends in Fig. 6B are observed here as well. The variance of the systems appears to increase as the smallest diffusion coefficient decreases. The systems also show the same tendency to form groups according to the smallest diffusion coefficient in the pair. There are also some very noticeable differences. The systems with a value of $1.0\cdot10^{-6}$ cm^2 s^{-1} for the smallest diffusion coefficient are linear. These systems equilibrate quickly and show no deviation from the trend expected from equilibrium theory. However, the systems that have a value of $1.0\cdot10^{-7}$ cm^2 s^{-1} for the smallest diffusion coefficient show slight curvature over short times, but become linear over long times. These systems reach steady state over the course of the simulation and behave as theory predicts. The systems with a value of $1.0\cdot10^{-8}$ cm^2 s^{-1} for the smallest diffusion coefficient initially show curvature and appear to reach a linear relation-

ship with time, but with a steeper slope. This greater dependence on time is believed to occur because the systems do not reach steady state within the time simulated (see below). The increased slope indicates that the zones broaden more than predicted by equilibrium theories because of the slow mass transfer kinetics of the second site.

The third moments in time and distance are presented in Figs. 6C and 7C, respectively. The third moments display trends similar to those of the second moments in both time and distance. The third moments in time are linear, whereas those in distance are not. For both time and distance domains, a decrease in the diffusion coefficient causes an increase in the third moment or asymmetry. It appears that the smallest diffusion coefficient is the controlling factor for the asymmetry, just as it was for the variance. It is interesting to note again that the third moments in time and distance are opposite in sign. The moments in time as a function of distance are positive (tailing profiles) while the moments in distance as a function of time are negative (fronting profiles).

3.3. Effect of differences in interfacial resistance to mass transfer

The final parameter studied is the barrier to mass transport across the interface between the fluid and surface phases. The *a* parameter in Eqs. (2a) and (2b) is maintained constant at 1.0 for one surface site, while the other site is varied from 1.0 to 0.001. The steady-state distribution of molecules between the surface and fluid phases as well as the mass transfer rate constants for these systems are recorded in Table 3. The ratio of the number of molecules in the surface and fluid phases appears to be similar for all of these systems. This implies that the steady-state behavior is not affected by the *a* parameter. However, the kinetics show a reduction in the rate constants as the *a* parameter is reduced. This indicates that as the resistance to mass transfer increases (*a* decreases), the rate of mass transfer across the interface decreases. As the *a* parameter is reduced to 0.001, the systems appear to change from single exponential kinetics to biexponential kinetics. This change in kinetic behavior can be seen in the values of the square of the correlation coefficient (R^2) of the fit to Eq. (3) as well as the characteristic times. The values of T_{50} show a steady increase as the *a* parameter decreases, but T_{90} and T_{95} show more substantial changes for the value of 0.001. This trend in the characteristic times indicates that the long-time response becomes dominated by the slow mass transfer of the surface site with the small value for the *a* parameter, while the short time behavior is dominated by the faster mass transfer of the other site.

The effect of the barrier to interfacial mass transfer on the fluid dynamic behavior can be seen in Fig. 8. This figure shows the zone profiles for the systems presented in Table 3 at columns lengths of 0.1 to 5.0 cm. Each system shows a decrease in the height of the zone profile, an increase in the width, and a decrease in the asymmetry as the column length increases. This is the same trend that is seen in the previous studies (Figs. 2 and 5) as well as for systems with homogeneous surfaces [37,42]. It can be seen that the asymmetry in the zone profile at 5.0 cm increases as the two values of the *a* parameter

Table 3
Rate constants (k_{fs}, k_{sf})[a], characteristic times (T_{50}, T_{90}, T_{95}), and steady-state distributions ($\tilde{N}_s/\tilde{N}_f$) for mass transfer processes as a function of the interfacial resistance to mass transfer (*a*)[b]

a_1	a_2	$\tilde{N}_s/\tilde{N}_f$	k_{fs}/k_{sf}	k_{fs} (s^{-1})	k_{sf} (s^{-1})	R^2	T_{50} (s)	T_{90} (s)	T_{95} (s)
1.0	1.0	1.008±0.005	0.992±0.003	0.370±0.006	0.373±0.006	0.965±0.001	0.75±0.01	3.93±0.09	5.3±0.2
1.0	0.1	0.998±0.007	0.995±0.002	0.37±0.02	0.37±0.02	0.924±0.004	0.83±0.02	3.6±0.1	4.8±0.3
1.0	0.01	0.993±0.010	0.985±0.008	0.23±0.02	0.24±0.02	0.963±0.008	1.53±0.07	6.7±0.1	9.23±0.03
1.0	0.001	0.986±0.006	0.880±0.008	0.099±0.003	0.112±0.004	0.77±0.01	2.33±0.03	37.2±0.6	55±9

[a] Determined by nonlinear regression according to Eq. (3) with square of the correlation coefficient R^2.

[b] Simulation conditions: $N=10\,000$; $t=1.0\cdot10^{-3}$ s; $T=20\tau$; $R_f=2.0\cdot10^{-3}$ cm; $R_s=8.28\cdot10^{-4}$ cm; $D_f=1.0\cdot10^{-5}$ cm^2 s^{-1}; $D_{s,1}=D_{s,2}=1.0\cdot10^{-7}$ cm^2 s^{-1}; $P_1=P_2=0.5$; $K_1=K_2=1.0$.

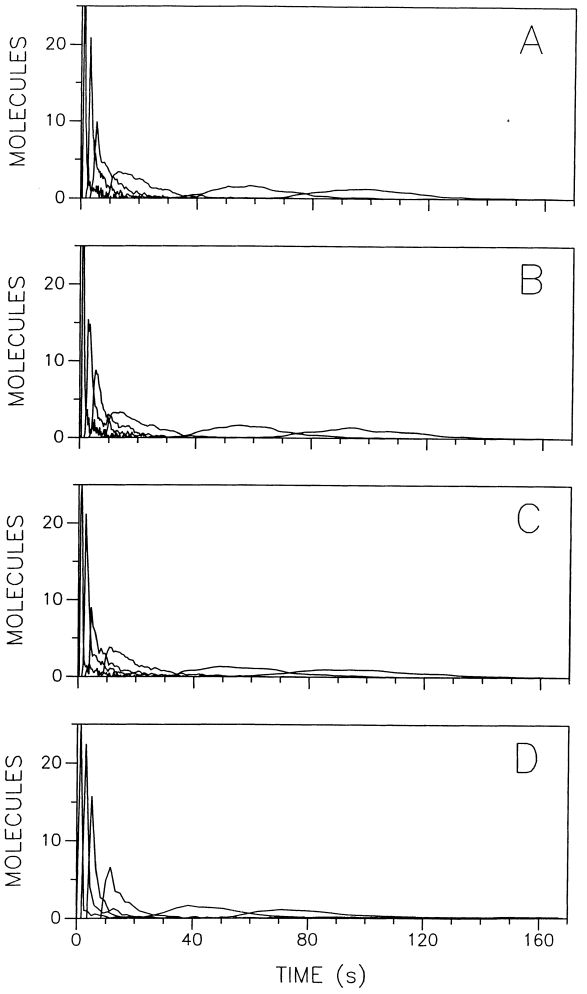

Fig. 8. Zone profiles for systems with laminar flow and two partition sites with (A) $a_1 = a_2 = 1.0$; (B) $a_1 = 1.0$, $a_2 = 0.1$; (C) $a_1 = 1.0$, $a_2 = 0.01$; (D) $a_1 = 1.0$, $a_2 = 0.001$. Simulation conditions: $N = 1000$; $t = 5.0 \cdot 10^{-5}$ s; $R_f = 2.0 \cdot 10^{-3}$ cm; $R_s = 8.28 \cdot 10^{-4}$ cm; $L = 0.1$, 0.2, 0.5, 1.0, 2.0, and 5.0 cm; $v = 0.1$ cm s^{-1}; $D_f = 1.0 \cdot 10^{-5}$ cm^2 s^{-1}; $D_{s,1} = D_{s,2} = 1.0 \cdot 10^{-7}$ cm^2 s^{-1}; $P_1 = P_2 = 0.5$; $K_1 = K_2 = 1.0$.

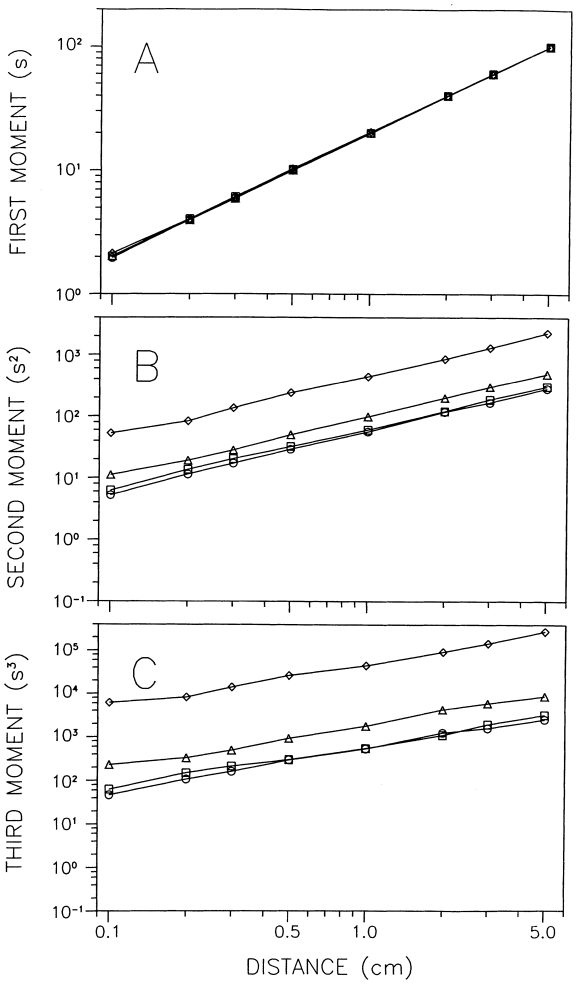

Fig. 9. The calculated (A) first moment, (B) second moment, and (C) third moment in time as a function of distance for systems with (○) $a_1 = a_2 = 1.0$; (□) $a_1 = 1.0$, $a_2 = 0.1$; (△) $a_1 = 1.0$, $a_2 = 0.01$; (◇) $a_1 = 1.0$, $a_2 = 0.001$. All other conditions as in Fig. 8.

diverge. The asymmetry is most noticeable for the system with $a_1 = 1.0$ and $a_2 = 0.001$, since it has the largest difference in the a parameter.

The moments of these systems in time and distance are shown Figs. 9 and 10, respectively. The first moments in time as a function of distance (Fig. 9A) are linear and equal in magnitude. This indicates that the a parameter does not affect the mean elution time. The first moments in distance as a function of time (Fig. 10A) are linear but show differences in magnitude, especially at short times. The magnitude of the first moments increases with a decrease in the a parameter and the corresponding mass transfer rate (Table 3). This implies that the differences in magnitude are the result of the time required for the mass transfer processes in the system to reach steady state. All of these observations are similar to those in the studies of diffusion coefficient discussed above.

The second moments shown in Figs. 9B and 10B increase as the values of the a parameter for the two sites diverge. However, the effect of the slow mass

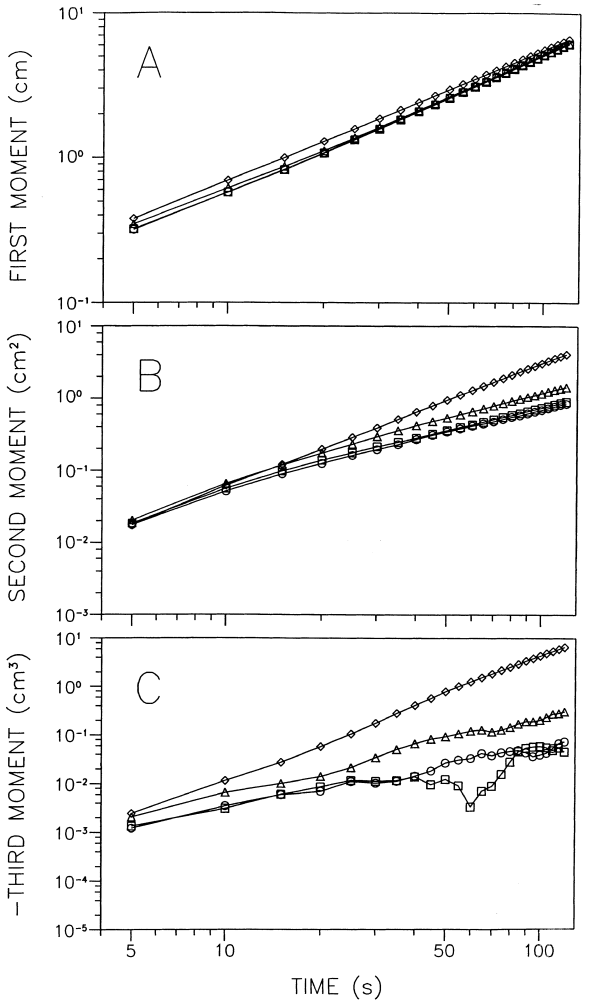

Fig. 10. The calculated (A) first moment, (B) second moment, and (C) third moment in distance as a function of time for systems with (○) $a_1 = a_2 = 1.0$; (□) $a_1 = 1.0$, $a_2 = 0.1$; (△) $a_1 = 1.0$, $a_2 = 0.01$; (◇) $a_1 = 1.0$, $a_2 = 0.001$. All other conditions as in Fig. 8.

transfer appears different in the time and distance domains. Fig. 9B shows linear correlation between the second moments and the column length, indicating that the systems are at steady state. However, Fig. 10B shows a nonlinear correlation between the second moment and time. The system with $a_1 = 1.0$ and $a_2 = 0.01$ shows curvature, and the system with $a_1 = 1.0$ and $a_2 = 0.001$ has a steeper slope than the other systems. Also, the second moments in Fig. 10B are initially similar in magnitude and then diverge as time increases. This implies that the initial response of the systems is controlled by the site with fast mass transfer ($a = 1.0$), and that the long-time behavior of the systems is controlled by the site with slower mass transfer. This trend supports the conclusion that the mass transfer of the systems becomes biexponential in character as the two values of the a parameter diverge. These trends in the second moments are similar to those for the diffusion coefficient described above.

The third moments shown in Figs. 9C and 10C increase as the values of the a parameter for the two sites diverge. The greatest asymmetry is produced by the highest barrier to interfacial mass transfer (smallest value of a). The third moments follow the same trends as described for the second moments above. The moments in time are a linear function of distance (Fig. 9C). The third moments in distance as a function of time (Fig. 10C) all appear to begin with comparable values, and then diverge as time increases. This indicates that the systems are equivalent initially, but become different at long time as the site with slow mass transfer becomes dominant. The moments also show nonlinear trends with time, especially for the system with $a_1 = 1.0$ and $a_2 = 0.001$.

4. Discussion

The systems studied in this report show the effects of multiple sites on the partition mechanism in chromatography. Differences in the partition coefficient of n different sites creates a system that responds as a homogeneous system with an average partition coefficient defined as:

$$K_{\text{avg}} = \sum_{i=1}^{n} P_i K_i \tag{11}$$

However, differences in either the surface-phase diffusion coefficient or the interfacial resistance to mass transfer cause the system to behave as reversible first-order reactions in competition, rather than a single reversible first-order reaction. These changes in the mass transfer kinetics cause the second and third moments to vary from those of a system with a homogeneous surface phase. These observations agree with previous work on the mass transfer rates

of diffusion-limited systems [42]. The mass transfer rate constants k_{fs} and k_{sf} are related to the system parameters by:

$$k_{fs} = \left[\frac{K(2R_fR_s + R_s^2)}{R_f^2 + K(2R_fR_s + R_s^2)}\right]\left(\frac{1}{D_f} + \frac{1}{D_s}\right)^{-0.5} \times \left(\frac{\pi R_f}{D_f} + \frac{\pi R_s}{D_s}\right)^{-0.5}\left[\frac{(R_f + \pi R_s)^2}{R_f^{1.5} R_s^2}\right] \quad (12)$$

$$k_{sf} = \left[\frac{R_f^2}{R_f^2 + K(2R_fR_s + R_s^2)}\right]\left(\frac{1}{D_f} + \frac{1}{D_s}\right)^{-0.5} \times \left(\frac{\pi R_f}{D_f} + \frac{\pi R_s}{D_s}\right)^{-0.5}\left[\frac{(R_f + \pi R_s)^2}{R_f^{1.5} R_s^2}\right] \quad (13)$$

From these equations, it is possible to show the dependence of the characteristic time $\tau = 1/(k_{fs} + k_{sf})$ associated with Eq. (3) on the partition coefficient and the surface-phase diffusion coefficient. It can easily be shown that the partial derivative of τ with respect to K is zero [42]. Thus, the mass transfer of the system is not dependent on the partition coefficient of the individual sites. This explains the independence of τ with respect to the partition coefficient already observed in the kinetic and fluid dynamic results presented above (Table 1 and Figs. 2–4). The systems with different partition coefficients behave identically to a single-site system with a partition coefficient equal to K_{avg}. The logarithmic graphs of the statistical moments are linear with a slope of 1. This indicates that the systems behave as would be expected for a system with a single site at steady state.

The partial derivative of τ with respect to D_s, however, is not zero [42]. Unlike the partition coefficient, the surface-phase diffusion coefficient affects the rate of mass transfer to and from the interface. Therefore, changes in the surface-phase diffusion coefficient will change the value of τ. This is apparent in the kinetic and fluid dynamic data presented above for systems with different diffusion coefficients (Table 2 and Figs. 5–7). As the difference in the diffusion coefficient of the individual sites increases, the difference in τ increases. Once the difference in τ is sufficiently large, the system shows biexponential kinetics for mass transfer between the fluid and surface phases. Accordingly, the multiple-site system shows greater deviations from the expected response of a single-site system as the difference in the diffusion coefficient of the individual sites increases. The most noticeable consequence of this deviation is the curvature in the second and third moments in Fig. 7. The second and third moments of systems with $1.0 \cdot 10^{-7}$ cm^2 s^{-1} for the smallest diffusion coefficient initially exhibit a slope of 2 that gradually decreases to 1 on the logarithmic graphs as time increases. The second and third moments of systems with $1.0 \cdot 10^{-8}$ cm^2 s^{-1} for the smallest diffusion coefficient exhibit a slope of 2 for the entire simulation time. This square dependence of the second moments on time can be explained by the fact that the two partition sites cause a spatial separation that is similar to that described by Golay and Atwood [43]. Their work describes a non-equilibrium phenomenon in which there is a group of molecules near the wall with zero velocity and a group of molecules in the center of the open tube with a velocity close to the maximum for the laminar profile. This distribution initially causes a zone profile with a ''boxcar'' shape having a variance that is proportional to the time squared. The profile described by Golay and Atwood is transient, and disappears quickly since the open tube has a very small volume of zero velocity. The systems simulated in this study have a stationary phase that produces two average velocities of the zone because of the different diffusion coefficients. This condition is probably transient as well but, because the mass transfer within the systems is slow, it requires more time to reach steady state than is simulated herein. The square dependence of the third moment on time further indicates that the systems are not at steady state.

The kinetic and fluid dynamic response of the system to differences in interfacial resistance to mass transfer appears to be similar to differences in diffusion coefficient. This indicates that the changes in mass transfer rate arising from changes in the a parameter affect the system in the same manner as those arising from changes in the diffusion coefficient. While it is possible to determine from the system response whether multiple sites with different mass transfer properties exist, the exact number and nature of those sites cannot be determined.

This work also demonstrates the inherent difference between the statistical moments in the time and

distance domains. For the data collected at a specified time, each molecule has the same amount of time to interact with the fluid and surface phases. This is different from the data collected at a specified distance, where each molecule has the same amount of time in the fluid phase but different total amounts of time. At steady state, the moments in time and distance are related to each other through the average velocity of the solute zone in the following manner:

$$\frac{M_{n,l}}{M_{n,t}} = \left(\frac{v}{1+K\beta}\right)^n \tag{14}$$

From this equation, it is evident that the higher moments are the most sensitive indication of the steady state. This expectation is verified by comparison of Figs. 6 and 7 or Figs. 9 and 10. When the system is not at steady state, the average velocity of each molecule is not equal to the average velocity of the zone and Eq. (14) is not satisfied. The moments in time and distance hold different information about a system that is not at steady state and, therefore, do not have a simple relationship to each other.

5. Conclusions

A new theoretical model has been applied to partition chromatography to study the effects of multiple surface sites. This model follows individual molecules through three-dimensional space, allowing independent interactions with the surface phase. There are many benefits to this kind of simulation. First, this model makes no assumptions about the relative contribution to mass transfer from the processes of diffusion, convection, and interaction with the surface phase. It is not necessary to neglect or to combine any of these processes in order to make the model tractable, as in the case of the mass balance approach. Thus, a detailed and unified model is available to study heterogeneous surfaces over a wide range of mass transfer rates.

Second, each molecule interacts independently with the surface, and any correlation between the different surface sites can be studied without prior knowledge or assumptions. This paper has shown that a heterogeneous system with differences in partition coefficient is indistinguishable from a homogeneous system with the same effective partition coefficient. Differences in the surface-phase diffusion coefficient or the interfacial resistance to mass transfer, however, result in different kinetic and fluid dynamic responses.

Finally, this model provides a wealth of information. Since the algorithms in the simulation are applied to an ensemble of molecules, it is possible to obtain molecular-level information as well as macroscopic information. The mass transfer curves, zone profiles, and statistical moments can easily be obtained from the same simulation. Thus, it is possible to associate the kinetic regime of the mass transfer curve with the curvature observed in the statistical moments. It is also possible to compare the time and distance moments to determine when the fluid dynamics of the system have reached steady state. The results presented herein suggest that the steady state is achieved when the ratio of the statistical moments in the time and distance domains is related to the average velocity of the solute zone, as given in Eq. (14). The findings for this simple two-site system suggest that further study by this method will be beneficial for more complicated systems.

Acknowledgements

This research was supported by the US Department of Energy, Office of Basic Energy Sciences, Division of Chemical Sciences, under contract No. DE-FG02-89ER14056. P.E.K. acknowledges receipt of the Dow Chemical Co. Graduate Fellowship from the Department of Chemistry, Michigan State University, and a summer research fellowship from the American Chemical Society, Division of Analytical Chemistry, sponsored by the Dow Chemical Foundation.

References

[1] G. Taylor, Proc. Roy. Soc. London Ser. A 219 (1953) 186.
[2] R. Aris, Proc. Roy. Soc. London Ser. A 235 (1956) 67.
[3] S. Golshan-Shirazi, G. Guiochon, in: F. Dondi, G. Guiochon (Eds.), Theoretical Advancement in Chromatography and Related Separation Techniques, Kluwer, Amsterdam, 1992, p. 61.
[4] L. Lapidus, N.R. Amundson, J. Phys. Chem. 56 (1952) 984.

[5] E. Kucera, J. Chromatogr. 19 (1965) 237.
[6] M.J.E. Golay, in: D.H. Desty (Ed.), Gas Chromatography, Academic Press, New York, 1958, p. 36.
[7] P.J. Karol, Anal. Chem. 61 (1989) 1937.
[8] P.J. Karol, J. Chromatogr. 445 (1988) 207.
[9] P.J. Karol, J. Chromatogr. 550 (1991) 247.
[10] G.L. Frey, E. Grushka, Anal. Chem. 68 (1996) 2147.
[11] G. Gotmar, T. Fornstedt, G. Guiochon, J. Chromatogr. A 831 (1999) 17.
[12] J.C. Giddings, H. Eyring, J. Phys. Chem. 59 (1955) 416.
[13] J.C. Giddings, J. Chem. Phys. 26 (1957) 169.
[14] D.A. McQuarrie, J. Chem. Phys. 38 (1963) 437.
[15] J.C. Oxtoby, J. Chem. Phys. 51 (1969) 3886.
[16] J.C. Giddings, J. Chem. Phys. 31 (1959) 1462.
[17] K. DeClerk, T.W. Smuts, V. Pretorius, Sep. Sci. 1 (1966) 443.
[18] G.H. Weiss, Sep. Sci. 2 (1967) 551.
[19] G.H. Weiss, Sep. Sci. 5 (1970) 51.
[20] A. Cavazzini, M. Remelli, F. Dondi, J. Microcol. Sep. 9 (1997) 295.
[21] A. Cavazzini, M. Remelli, F. Dondi, A. Felinger, Anal. Chem. 71 (1999) 3453.
[22] G.P. Hilderbrand, C.N. Reilley, Anal. Chem. 36 (1964) 47.
[23] G.W. Pilgrim, R.A. Keller, J. Chromatogr. Sci. 11 (1973) 206.
[24] B.Y. Zhu, C.T. Mant, R.S. Hodges, J. Chromatogr. 594 (1992) 75.
[25] S. Heron, A. Tchapla, J. Chromatogr. A 725 (1996) 205.
[26] B. Buszewski, R.M. Gadzala-Kopiuch, M. Jaroniec, J. Liq. Chromatogr. Rel. Technol. 20 (1997) 2313.
[27] C.H. Lochmuller, A.S. Colborn, M.L. Hunnicutt, J.M. Harris, Anal. Chem. 55 (1983) 1344.
[28] Y. Bereznitski, M. Jaroniec, M.E. Gangoda, J. Chromatogr. A 828 (1998) 59.
[29] T.L. Beck, S.J. Klatte, L.A. Cole, J.G. Dorsey, J. Chromatogr. A 656 (1993) 317.
[30] R.E. Boehm, D.E. Martire, J. Phys. Chem. 84 (1980) 3620.
[31] D.E. Martire, R.E. Boehm, J. Phys. Chem. 87 (1983) 1045.
[32] I. Yarovsky, M.I. Aguilar, M.T.W. Hearn, J. Chromatogr. A 660 (1994) 75.
[33] I. Yarovsky, M.I. Aguilar, M.T.W. Hearn, Anal. Chem. 67 (1995) 2145.
[34] S.J. Klatte, T.L. Beck, J. Phys. Chem. 99 (1995) 16024.
[35] S.J. Klatte, T.L. Beck, J. Phys. Chem. 100 (1996) 5931.
[36] J.T. Slusher, R.D. Mountain, J. Phys. Chem. B 103 (1999) 1354.
[37] M.R. Schure, Adv. Chromatogr. 39 (1998) 139.
[38] V.L. McGuffin, P.E. Krouskop, D.L. Hopkins, in: J.F. Parcher, T.L. Chester (Eds.), Unified Chromatography, ACS Symposium Series No. 748, American Chemical Society, Washington, DC, 1999, p. 37, Chapter 4.
[39] V.L. McGuffin, P. Wu, J. Chromatogr. A 722 (1996) 3.
[40] D.L. Hopkins, V.L. McGuffin, Anal. Chem. 70 (1998) 1066.
[41] P. Wu, V.L. McGuffin, AIChE J. 44 (1998) 2053.
[42] V.L. McGuffin, P.E. Krouskop, P. Wu, J. Chromatogr. A 828 (1998) 37.
[43] M.J.E. Golay, J.G. Atwood, J. Chromatogr. 186 (1979) 353.